Study of pollutant emissions and dynamics of non-premixed turbulent oxygen enriched flames from a swirl burner

Toufik Boushaki, Nazim Merlo, Christian Chauveau, Iskender Gökalp

Study of emission pollutants and dynamics of non-premixed turbulent oxygen enriched flames from a swirl burner

Toufik Boushaki [a,b,*], Nazim Merlo [a], Christian Chauveau [a], Iskender Gökalp [a]

[a] *ICARE CNRS, 1C, Avenue de la Recherche Scientifique, 45071 Orléans, France*
[b] *University of Orléans, IUT, GTE, 45067 Orléans cedex 2, France*

Abstract

The paper investigates the emission pollutants and the dynamics of methane - oxygen enriched air turbulent non-premixed flames from a swirl burner. The burner's configuration consists of two concentric tubes with a swirler placed in the annular part supplying the oxidant. The injection of fuel is radial throughout holes in the central tube at the burner exit. This allows enhancing air-fuel mixing before the stabilization point of flame. The idea of oxygen enrichment of the air is related to the augmentation of CO_2 concentration in the flue gas to improve membrane capture approach of CO_2. Stereo-Particle Image Velocimetry is used to analyze the velocity flow fields. The measurements are performed for oxygen concentrations ranging from 21 % to 30 %, with swirl numbers from 0.8 to 1.4 and global equivalence ratio from 0.8 to 1. Results show that combustion noticeably affects the swirling motion and that tangential velocities rapidly decrease along the axial axis. Besides the recirculation mass flow ratio dramatically increases compared to non-reactive cases. Increasing global equivalence ratios increase the recirculation mass flow ratio contrary to oxygen enrichment effects. Fuel is injected into the highest turbulence level regions where the local mixing is enhanced, supporting the idea of a shift from a non-premixed flame towards a partially premixed one. The exhaust gas compositions are measured using gas analyzers. It is observed that NO_x emissions decrease when the global equivalence ratio increases. It suggests that CO_2 in the recirculated burned gases could be responsible for NO_x destruction at relatively high oxygen enrichment rates. Globally, the results show that the developed and characterized new burner configuration has a good potential to be used to stabilize non-premixed fuel and oxidant streams as partially premixed low emission flames with an increased concentration of CO_2 in the flue gases, by combining enhanced mixing and moderate oxygen enrichment of the air.

1. Introduction

The use of gaseous fuels for energy generation, such as natural gas but also more and more synthetic gases from various gasification processes, is growing worldwide. Gaseous fuels emit less CO_2 compared to coal or fuel oil and the recent rush to shale gas, for instance in the US but also soon in Europe, added to the development of large-scale coal gasification plants for example in China, will keep this resource alive for several decades [1]. In most gaseous fuel applications for industrial combustion, the diffusion or non-premixed combustion mode is preferred for obvious safety reasons [2]. This is all the more justified when hydrogen or hydrogenated fuels such as syngas, are used [3]. It is well known that the NO_x generation propensity of non-

premixed flames is higher compared to premixed flames [4]. When combining this emission problem with the safety issue mentioned above, an obvious solution is an innovative burner configuration which converts a non-premixed flame to a premixed or at least partially premixed one. Theoretically, such a burner should prevent any explosion risk by avoiding premixing the fuel with the oxidant before ignition and generate a premixed like flame after ignition. This paper discusses such a burner configuration which combines a swirling co-flow of the oxidant with a radial injection of the fuel [5-7].

Another issue today is the CO_2 capture from industrial flames. This constraint will become more stringent in the future and will be applied not only to very large power plants but also to medium scale industrial combustion systems. Post-combustion CO_2 capture is today a costly process when chemical capture solutions are applied [8]. Oxy-fuel combustion is an elegant solution but disadvantaged by the energetic penalty of oxygen generation. Post-combustion capture of CO_2 using physical processes such as membranes appear as a viable solution at least until low-cost oxygen production technologies is available [9, 10]. Membrane capture systems of CO_2 require, however, CO_2 concentrations not smaller than 20 % in flue gas [11]. This can be obtained by partial oxygen enrichment of the reactive mixture [12, 13]. One negative aspect of this approach is obviously its NO_x enhancing effect [14, 15]. Combining an innovative burner configuration allowing enhanced mixing with a moderate oxygen enrichment to enable CO_2 capture by membranes is the challenge of the present work.

In the following paragraphs, the burner configuration is first described and characterized by stereo-PIV under non-reacting and reacting conditions. Instantaneous and averaged OH images are also obtained to help characterize the flame structure. Post flame emission measurements of CO_2, CO and NO_x are performed to discuss the merits of the developed burner configuration and the future research paths for its improvement.

2. Experimental system

2.1. Burner and flame configurations

The burner used in this study consists of two concentric tubes with a swirler placed in an annular part supplying the oxidant flow (air or oxygen-enriched air) as shown in Fig. 1a. Eight guide vanes are designed with various vane angles to induce swirl intensity variations. The central pipe delivers radially the fuel (methane) through eight holes symmetrically distributed on the periphery of the tube, just below the burner exit plane. Note that this configuration of swirl burner is high 3D and not axisymmetric. The fuel injection mode strongly determines the flame

type [6]. The outer annular part diameter and the related radius are defined by D_b and R_b respectively. Figures 1b-1c show the variations of flame shapes with the axial and the transverse (or radial) methane injection modes. When the axial methane injection is used, a long yellow typical turbulent non-premixed flame is obtained for which slight increases of air flow rates eventually lead to flame blowout. When the radial methane injection is applied, a tulip-shaped blue flame is obtained. Thus, the combustion mode is changed from diffusion-type to partially premixed type swirling flames. In the present work, the radial injection of fuel is used to enhance mixing at the near field of the burner exit. Variations of the flame shape with oxygen content are depicted in Figures 1d-f.

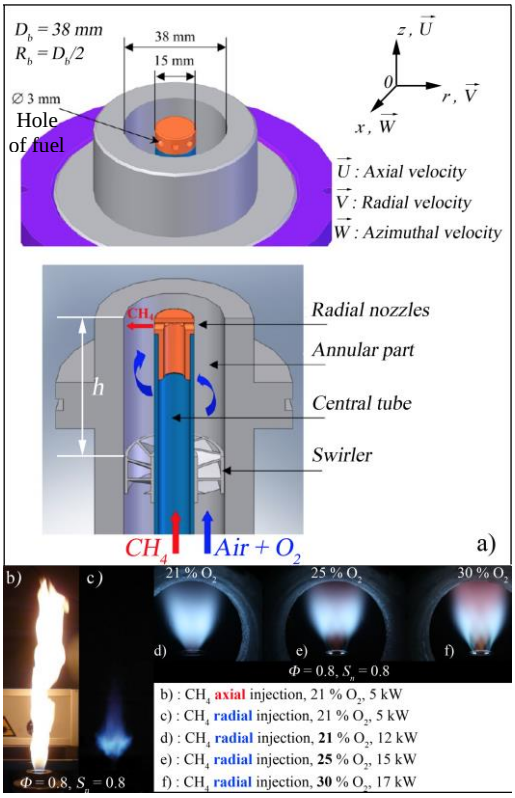

Fig. 1. Burner configuration (a) and flame images for two fuel injection modes and various oxygen enrichment rates (b-f).

The degree of swirl for rotating flows is usually characterized by the nondimensional swirl number S_n which represents the ratio of the axial flux of radial momentum G_x and the axial flux of axial momentum G_z [16]:

$$S_n = \frac{G_x}{G_z R} \tag{1}$$

The geometrical swirl number S_n related to this configuration is defined as [16]:

$$S_n = \frac{1}{1-\psi} \cdot \left(\frac{1}{2}\right) \cdot \frac{1-(R_h/R)^4}{1-(R_h/R)^2} \tan\alpha_0 \tag{2}$$

where ψ is the blockage factor and α_0 is the vane angle. R and R_h are nozzle and vane pack hub radii respectively. The swirler position above the burner exit plane is indicated by h and fixed at 60 mm in this work. The experiments are conducted with a square cross-section chamber of 48 x 48 cm^2 and 1 m height operating at atmospheric pressure. The walls of the combustion chamber are water-cooled on the outside and refractory-lined inside. Six windows are placed in each face of the chamber allowing optical access to all the potential flame zones. A global equivalence ratio, Φ, can be defined as the molar ratio of methane and oxidant flows at injection to the molar ratio of methane and oxidant at stoichiometric conditions. An oxygen-air mixture is employed as the oxygen-enriched oxidizer flow. Mass flow rates of air, oxygen and fuel are regulated by thermal mass flow controllers.

The measurements are performed for oxygen concentrations ranging from 21 to 30 % in volume, with swirl numbers of 0.8 and 1.4, and for global equivalence ratios of 0.8, 0.9 and 1. Table 1 summarizes the mass flow rates of the reactants, Reynolds number of the oxidizer and the burner power as a function of the oxygen enrichment and equivalence ratio. It can be noticed that from 21 to 30% of O_2 the volumetric flow rate of the oxidizer (air +O_2) kept constant for varying oxygen enrichment rates for a given global equivalence ratio. The mass flow rate (and hence the oxidizer Reynolds number), however, varies a little because the little variation of the density with O_2 enrichment (Table 1). As a consequence the fuel flow rates vary.

Table 1. Burner operating conditions for various global equivalence ratios and oxygen enrichment rates.

Φ	O_2 vol. (%)	$\dot{M}_{Air}$ (g/s)	$\dot{M}_{O_2}$ (g/s)	$\dot{M}_{CH_4}$ (g/s)	Re_{OX}	P_{th} (kW)
0.8	21	5.14	0.00	0.24	7320	12.2
	24	5.01	0.21	0.28	7340	13.9
	25	4.96	0.30	0.29	7360	14.5
	27	4.82	0.46	0.31	7381	15.7
	30	4.54	0.67	0.35	7423	17.4
0.9	21	5.14	0.00	0.27	7320	13.7
	24	5.01	0.21	0.28	7340	15.7
	25	4.96	0.30	0.33	7360	16.3
	27	4.82	0.46	0.35	7381	17.6
	30	4.54	0.67	0.39	7423	19.5
1.0	21	5.14	0.00	0.30	7320	15.2
	24	50.1	0.21	0.28	7340	17.4
	25	4.96	0.30	0.36	7360	18.1
	27	4.82	0.46	0.39	7381	19.6
	30	4.54	0.67	0.44	7423	21.7

2.2. Measurement techniques

Because of the strongly three-dimensional characteristics of the flow field structures, Stereo Particle Image Velocimetry (S-PIV) is used to gain insight into the flow field under non-reacting and reacting conditions. A double-pulsed Nd:YAG laser (Minilite 25 mJ/pulse) with a wavelength of 532 nm operating at 10 Hz is used as the light source. Synchronization between the cameras and the laser is achieved by means of a TSI synchronizer Laser Pulse 610035. The mean time between two successive frames is 25 μs. An optical system with a plano-convex cylindrical lens (focal length of 12.7 mm) and a spherical lens (focal length of 592 mm) transforms the laser beam into a laser sheet of about 500 μm thickness and about 100 mm height at the center of the measurement window. The two cameras mounted on Scheimpflug adapters (TSI Powerview Plus 4MP, 12-bit output and 2048 x 2048 pixels^2) are oriented perpendicular to the laser sheet. They are located on the same side of the latter. The angle between the two cameras is limited to 30° because of optical access limitations. Band-pass filters centered at 532 nm with a 10 nm bandwidth (50 %) are used to collect Mie particle scattering. A precision-machined twin level calibration target with dot pattern, perfectly centered over the burner inner diameter, is used for calibration. A host computer captures 500 pairs of image frames for each camera continuously with each frame covering a flow area of about 115 mm (width) x 95 mm (height). Nikon AF Micro-Nikkor 105 mm F/2.8 lenses are used to collect the PIV signal. TSI Insight 3G software is used to analyze S-PIV images and a background extraction scheme is applied to reacting case images as pre-processing step. The Al_2O_3 particles used for seeding the flow are 0.5-1 μm in diameter. Considering 32×32 pixels interrogation cells, a magnification ratio of 0.11 and 50% overlap grid spacing, a typical spatial resolution achieved for the velocity vector grid is 1.1 mm in both directions.

Concentrations of exhaust gases such as NO_x, CO, CO_2, and O_2 are measured by a HORIBA PG250 multi-gas analyzer on a dry basis. The uncertainties in the measurements of pollutant emissions are around 1% of the measured concentration. OH* chemiluminescence technique is used to visualize the reaction zone and to measure the liftoff heights and flame lengths [17, 18]. Uncertainties are estimated as within 5% for the average flame height. Details about the two techniques are provided in [5].

3. Results and Discussions

3.1. Flame effects on the IRZ and the swirling motion

For safety reasons the experiments under non-reacting conditions are performed using nitrogen instead of methane while keeping constant the momentum of the radial jets. Contours of axial U

and tangential W velocities up to 2.5*D* downstream of the jet development (plotted respectively in Fig. 2a and 2b) show the mean flow fields in non-reacting and reacting conditions for the air case with a swirl number S_n = 0.8 and a global equivalence ratio Φ = 0.8. The investigated field is symmetrical about the line x = 0, shown as a dashed line in Figure 2. Therefore, only the left part, defined as x/R_b varying from 0 to -3, of the investigated field for both conditions is plotted in Fig. 2. Figure 2a highlights the axial expansion induced by combustion. As expected from the intense swirling flows, an internal recirculation zone (IRZ) is established for non-reacting and reacting conditions. Besides, the IRZ becomes larger, due to density changes resulting from combustion, and more intense for the reacting case compared to the non-reacting case. Figure 2b shows that the tangential velocity W rapidly decreases along the z-axis with a slight shift of the swirling motion towards the central axis downstream compared to the non-reacting flow case.

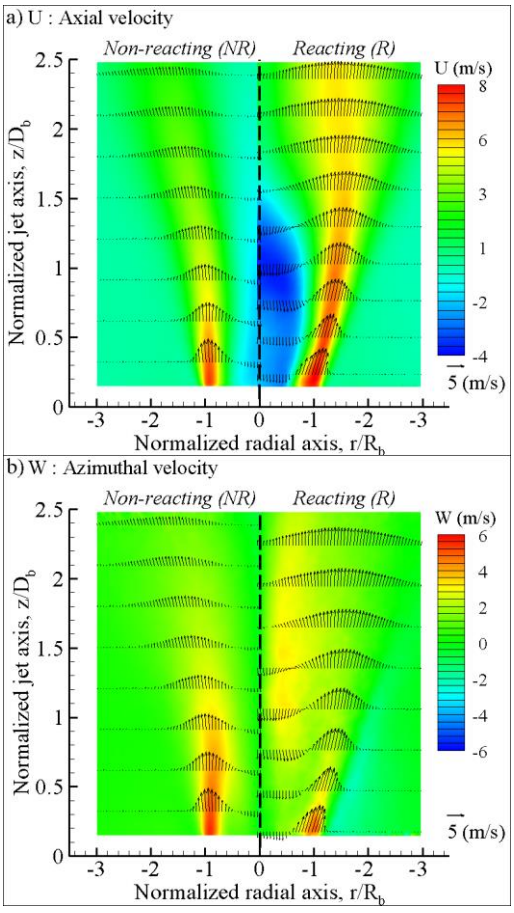

Fig. 2. Fields of axial (U) (a) and tangential (W) (b) velocities under non-reacting and reacting conditions: S_n = 0.8 and Φ = 0.8.

Figure 3 displays the radial profiles of the axial U and tangential W velocities at different heights from the burner, in the non-reacting and reacting flows for the air case with S_n = 0.8 and a global equivalence ratio Φ = 0.8. The entire investigated field is plotted in Fig. 3. For z / D = 0.3, namely before the flame front, the maximum axial velocity in non-reacting and reacting

conditions are quite similar between 7 and 8 m/s at maximum peak axial velocities. For $z / D = 1$, in the reaction zone, peak positive velocities are increased by 45 % compared to non-reacting velocities. Meanwhile, the reverse flow is also intensified. Reverse axial velocity decreases from -1 m / s to – 4 m / s at $z / D = 1$. Combustion impact on the ~~azimuthal~~ tangential velocity field tends to show that the intensity of the swirling motion is lower than the motion originally imposed to the oxidant flow [19] in non-reacting flows.

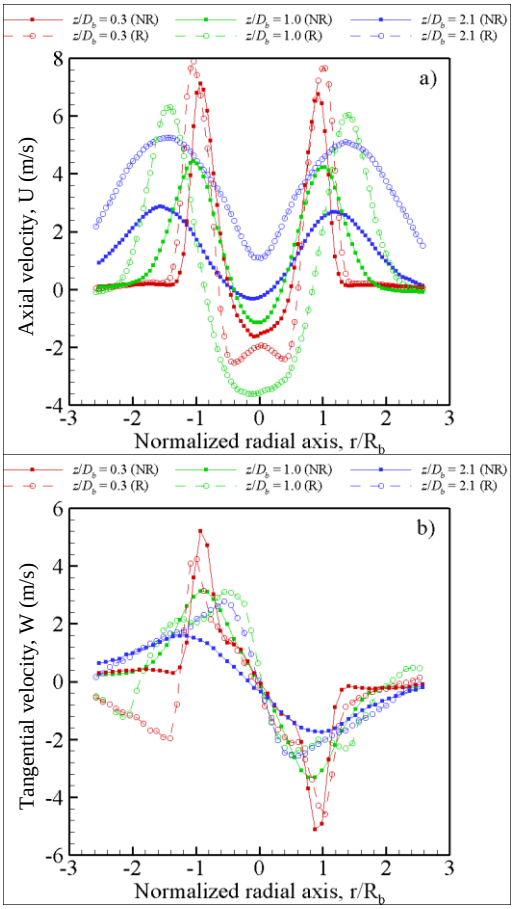

Fig. 3. Radial profiles of axial (a) and tangential (b) mean velocity in non-reacting and reacting swirling flows at various normalized axial stations: $S_n = 0.8$ and $\Phi = 0.8$.

IRZ plays a dominant role in determining the mixing quality of fuel-air for more complete combustion by recirculating the hot combustion products [20]. Figure 4a shows the recirculation mass flow ratio along the normalized jet axis for two swirl numbers $S_n = 0.8$ and 1.4, with two oxygen enrichment rates 21 and 30 %, under non-reacting (NR) and reacting conditions ®. M_r defines the recirculated mass flow inside the jet and M_0 refers to the input mass flow at z/D_b. The largest differences are noticed between the non-reacting flow and the reacting case where the maximum value of M_r/M_0 increases from 0.18 to 0.6 with a peak shift downstream. In addition, increasing oxidant content leads to lower the maximum recirculation mass flow ratio from 0.6 to 0.48 when the oxygen content increases from 21 to 30 %. Increasing swirl intensity improves

mass flow recirculation inside the non-reacting flow. Nevertheless, in reacting conditions, since combustion tends to lower swirl effects, differences between the two swirl numbers S_n = 0.8 and S_n =1.4 seem to be insignificant. Figure 4b highlights the global equivalence ratio effects on the recirculation mass flow rate for a swirl number S_n = 1.4 and 25 % O_2 in the oxidant. Increasing the global equivalence ratio from 0.8 to 1 leads to weak increase of the maximum values of recirculation mass flow ratio from 0.55 to 0.65. On the integral values of the recirculation mass flow, there is also a week increase with the equivalence ratio. Although reverse flow intensification may lead to improve flame stability, flame liftoff investigations conducted in [5] show that the liftoff height increases with global equivalence ratio from 0.8 to 1. In the next section, the emissions results show the NOx reduction with equivalence ratio, which is induced by this increase of recirculation mass flow that decreases the flame temperature.

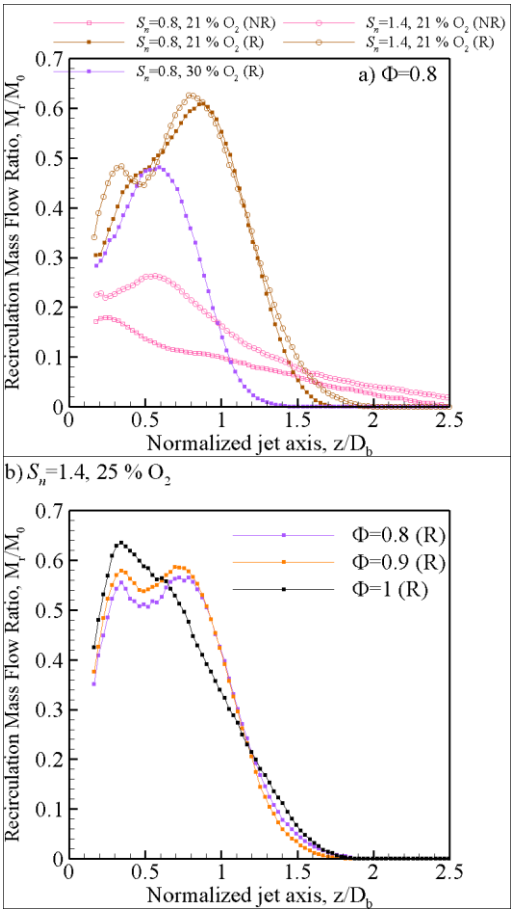

Fig. 4. Distribution of recirculated mass flow rate along the normalized jet axis for various swirl numbers, oxygen enrichment rates (a) and global equivalence ratios (b).

These measurements yield valuable information to better understand the large stability domain depicted in [5] for such a burner which takes fully advantage of swirling motions to enhance the mixing process and, therefore improve non-premixed flame stability.

3.2. Turbulence fields and flame front fluctuations

The normalized turbulent kinetic energy distribution, $k^{1/2}/U_{bulk}$, close to the burner exit indicates strong turbulent mixing in the jet development and the IRZ under reacting conditions. k represents the turbulent kinetic energy for the three velocity components. U_{bulk} refers to the computed velocity based on the sum of oxidant and fuel flow rates which flow inside the burner annular part without the swirler. Contours of $k^{1/2}/U_{bulk}$ are reported in Fig. 5a under non-reacting and reacting conditions with a S_n = 0.8 and a global equivalence ratio Φ = 0.8. It is observed that the methane is directly injected into the swirling flow where maximum turbulent kinetic energy takes place. As a result it creates favorable conditions for generating partially premixed flames. Figure 5b presents normalized turbulent kinetic energy profiles extracted from Fig. 5a. These profiles show that as a consequence of combustion the velocity fluctuations, especially the axial velocity fluctuations, increase significantly. Besides, the IRZ, which is typically a low velocity region, exhibits a level of turbulence twice larger than in the non-reacting flow in the vicinity of the burner exit.

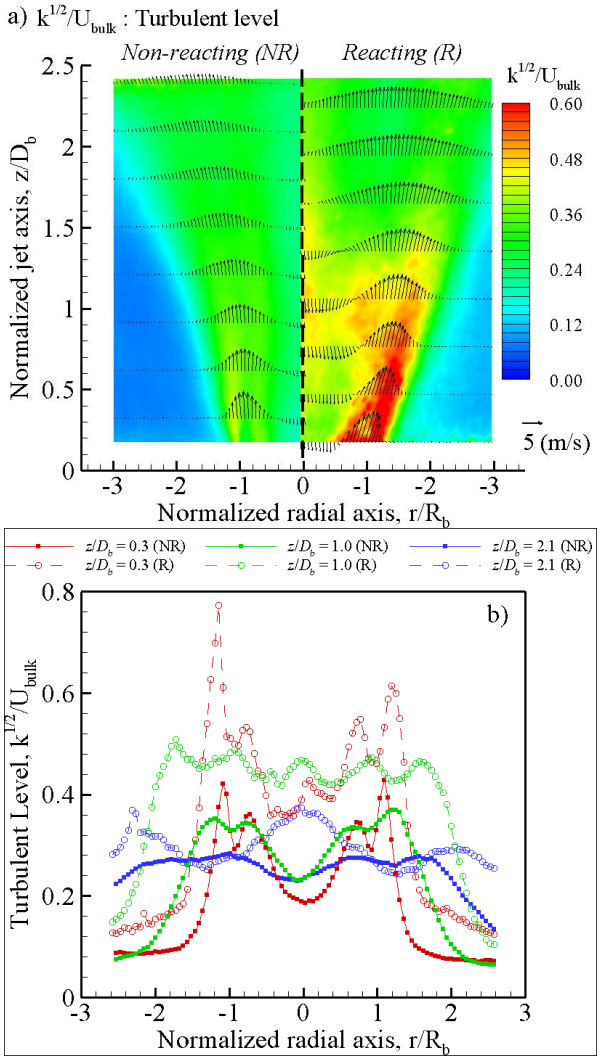

Fig. 5. Field of normalized turbulent kinetic energy (a) and extracted profiles (b) at various normalized axial stations for S_n = 0.8 and Φ = 0.8.

Turbulence levels may be related to flame front fluctuations which are obtained with OH* flame chemiluminescence. A threshold value, based on the inflection point determination, is applied to mean flame chemiluminescence images in order to detect the flame contours. As an example, normalized liftoff heights H_{lo}/D_b and tip flame positions L_f/D_b are given in Fig. 6 for 3 oxygen enrichment rates from 21 to 30 % with a swirl number S_n = 1.4 and global equivalence ratio Φ = 0.8. Further increases in oxygen enrichment rates result in decreases of the liftoff heights as well as the flame tip positions. Flame shapes evolve strongly with oxygen content. This also reveals that swirling flame stabilization process is strongly influenced by the reverse flow regions.

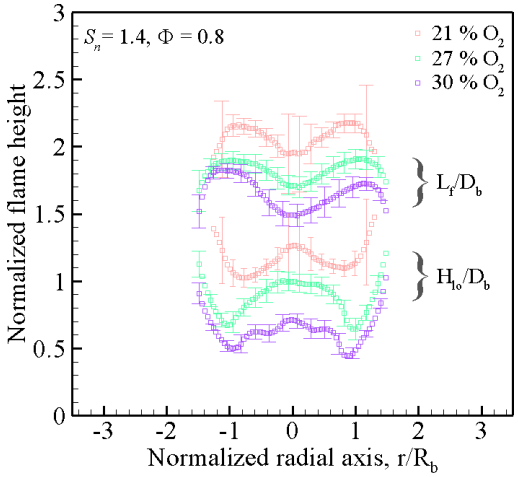

Fig. 6. Flame front heights and their fluctuations along the radial axis for various oxygen enrichment rates.

3.3. CO, NO_x and CO_2 emissions

The emission index of CO (EICO) and NO_x ($EINO_x$) are defined as the total grams of emissions produced when 1 kg of fuel is burned [21]. All measured emissions are on a dry basis and refer to the same oxygen content of 3 %. Figure 7a reveals the EICO evolutions with the global equivalence ratio with a swirl number S_n = 1.4. Increasing equivalence ratio dramatically decreases CO formation from 18 to 2 g / kg of CH_4 especially for low oxygen enrichment rates. This may be related to a higher recirculation mass ratio when the global equivalence ratio increases as depicted in Fig. 4b. As expected, oxygen enrichment leads to promote CO conversion into CO_2 [12]. Figure 7b highlights $EINO_x$ evolutions along the global equivalence ratio from 0.8 to 1 with S_n = 1.4 and three O_2 enrichments (21%, 24, 27 and 30%). Note that the measurement error is around 1% on average; however, in some cases it can reach about 10% as the case Φ=0.9 and Φ=1 with 30% O_2 where the values highly fluctuate.

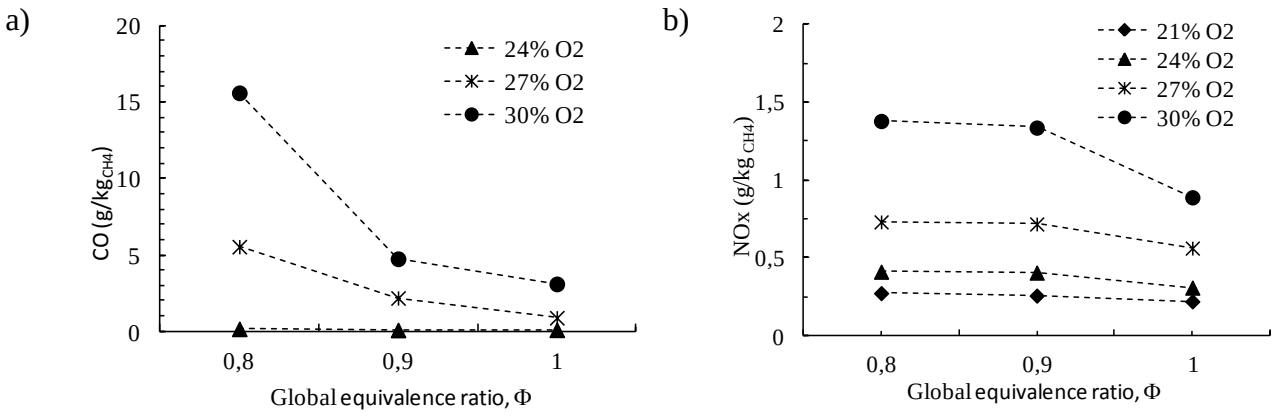

Fig. 7. EICO (a) and $EINO_x$ (b) and evolutions with global equivalence ratio for various oxygen enrichment rates and swirl number S_n = 1.4.

The NOx emissions increase with O_2 enrichment. This decrease is certainly due to the increase of flame temperature with O_2 addition via the thermal NO mechanism. The increase of equivalence ratio from 0.8 to 1 induces a decrease of NOx rate. For 24% of O_2 in the oxidant for example, NOx emissions decrease from 1.5 to 0.8 g / kg_{CH4} when the global equivalence ratio varies from 0.8 to 1. This result seems surprising because the temperature increases when equivalence ratio approaches the stoichiometry, which normally increases NOx emissions, if this is the thermal NO mechanism is primarily responsible for NOx formation. These results can be explained by the following reason: As equivalence ratio increases, the mole fraction of CO_2 in combustion products increases as shown in Figure 8. This increase of CO_2 emissions induces an increase in the amount of recirculated CO_2, which chemically increases the nitrogen oxide destruction [22]. In diffusion flames with recirculating burned gases, prompt NO and thermal NO react with CO_2 and decrease NOx emissions [15]. The decrease of the CO_2 amount in the recirculation zone led to higher NOx emissions. These tendencies were also found in the literature as [23].

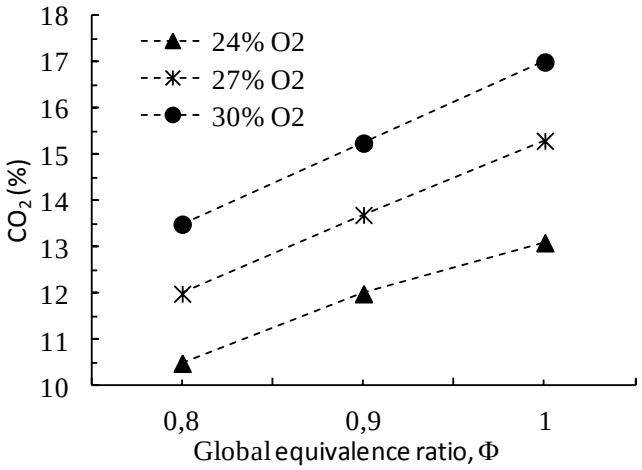

Fig. 8. CO_2 evolutions with global equivalence ratio for various oxygen enrichment rates and swirl number S_n = 1.4.

4. Conclusion

Characteristics of turbulent non-premixed swirling flames with oxygen enrichment are investigated in this paper. The emphasis is on emission pollutants (CO, NOx and CO_2) and velocity fields for several burner parameters as equivalence ratio, oxygen addition rate and swirl number. The mass flow recirculation ratio, the flame shape and the turbulent levels are investigated through comparisons between non-reacting and reacting flow fields. Results of velocity measurements show clearly the swirl effect with a recirculation zone and negative longitudinal velocity in the burner center. This central recirculation zone results to the presence of the swirler and central tube in the burner. The comparison between the non-reactive case and the reactive case indicates two main phenomena: First, a greater radial expansion of flow with a larger recirculation zone in the reactive case; second, a higher velocity in particular above the stabilization zone. Emission pollutant measurements reveal that the oxygen enrichment is vey advantageous for CO reduction and CO_2 augmentation; however, it is disadvantageous for NOx reduction. The rise of NOx is due to the increase of the flame temperature, which favors the formation of NOx by the thermal bath. But if the O_2 enrichment remains less 30%, the NOx rate is acceptable for standard values.

Acknowledgements

This work is supported by the ANR (Agence Nationale de la Recherche), project CO_2 Energicapt (ANR-10-EESI-0003). We thank Marc Morlat from Orleans University for comments that greatly improved the manuscript.

References

[1] L.M. Cathles, L. Brown, M. Taam, A. Hunter, Climatic Change, 113 (2012) 525-535.

[2] C.E. Baukal, The John Zink Hamworthy Combustion Handbook; 2nd ed., CRC Press, 2013.

[3] T. Lieuwen, V. Yang, R. Yetter, Synthesis gas combustion: fundamentals and applications, CRC Press, 2010.

[4] F. Cozzi, A. Coghe, Exp. Thermal Fluid Sci., 43 (2012) 32-39.

[5] N. Merlo, T. Boushaki, C. Chauveau, S. de Persis, L. Pillier, B. Sarh, I. Gökalp, Energy Fuels, 27 (2013) 6191-6197.

[6] A. Olivani, G. Solero, F. Cozzi, A. Coghe, Exp. Thermal Fluid Sci., 31 (2007) 427-436.

[7] T.S. Cheng, Y.C. Chao, D.C. Wu, T. Yuan, C.C. Lu, C.K. Cheng, J.M. Chang, Proc. Combust. Inst., 27 (1998) 1229-1237.

[8] T.F. Wall, Proc. Combust. Inst., 31 (2007) 31-47.

[9] E. Favre, R. Bounaceur, D. Roizard, Sep. Purif. Technol., 68 (2009) 30-36.

[10] D. Singh, E. Croiset, P.L. Douglas, M.A. Douglas, Energy Conversion Manag., 44 (2003) 3073-3091.

[11] B. Belaissaoui, G. Cabot, M.-S. Cabot, D. Willson, E. Favre, Chem. Eng. Sci., 97 (2013) 256-263.

[12] H.S. Zhen, C.W. Leung, C.S. Cheung, Applied Energy, 88 (2011) 2925-2933.

[13] J. Song, V. Zello, A.L. Boehman, F.J. Waller, Energy Fuels, 18 (2004) 1282-1290.

[14] H.Y. Kim, S.W. Baek, C.Y. Lee, Combust. Sci. Technol., 181 (2009) 1289-1309.

[15] J. Park, J.S. Park, H.P. Kim, J.S. Kim, S.C. Kim, J.G. Choi, H.C. Cho, K.W. Cho, H.S. Park, Energy Fuels, 21 (2007) 121-129.

[16] J.M. Beér, N.A. Chigier, Combustion Aerodynamics, Applied Science Publishers Ltd, 1972.

[17] D.S. Dandy, S.R. Vosen, Combust. Sci. Technol., 82 (1992) 131-150.

[18] S.H. Bae, H.D. Shin, Energy Fuels, 23 (2009) 5338-5348.

[19] S.A. Beltagui, A.M.A. Kenbar, N.R.L. Maccallum, Exp. Thermal Fluid Sci., 6 (1993) 147-156.

[20] A.K. Gupta, D.G. Lilley, N. Syred, Swirl Flows, Abacus Press, 1984.

[21] R.-H. Chen, J.F. Driscoll, Proc. Combust. Inst., 23 (1991) 281-288.

[22] H. Watanabe, T. Marumo, K. Okazaki, Energy Fuels, 26 (2012) 938-951.

[23] S. Yon, J.-C. Sautet, T. Boushaki, Energy Fuels, 26 (2012) 4703-4711.